Journal of Membrane Science 350 (2010) 378–386

Contents lists available at ScienceDirect

Journal of Membrane Science

journal homepage: www.elsevier.com/locate/memsci

A simulation study of the effect of operating and design parameters on the performance of a water gas shift membrane reactor

Panagiotis Boutikos[a], Vladimiros Nikolakis[b,*]

[a] Department of Chemical Engineering, University of Patras, Greece
[b] Institute of Chemical Engineering & High Temperature Chemical Processes, Foundation for Research and Technology Hellas (FORTH/ICE-HT), Stadiou Str, PO Box 1414, 26504 Patras, Greece

ARTICLE INFO

Article history:
Received 28 September 2009
Received in revised form
28 December 2009
Accepted 7 January 2010
Available online 14 January 2010

Keywords:
Water gas shift
Membrane reactor
Reactor design

ABSTRACT

The goal of this work is to understand the effect of the relative values of membrane permselectivity, permeation flux and reaction rate on the performance of a water gas shift membrane reactor. This was achieved by simulating the operation of an isothermal tube–shell reactor. Its performance was evaluated based on the CO conversion and H_2 recovery, as well as the permeate and retentate H_2 molar fractions. The maximum enhancement of CO conversion has been observed when the Damkhöler number (*Da*) is almost equal to the permeation number (*Pe*). Improvements in CO conversion can be achieved even when membranes with relatively low permselectivity values (~10) are used. Further increase of permselectivity primarily increased the purity of the H_2 rich stream. The utilization of CO_2 selective instead of H_2 selective membranes could improve CO conversion only if the CO_2 content of the feed is higher than that of H_2. Finally, simulations using rate expressions that correspond to different detailed reaction mechanisms resulted only in slight differences in reactor performance.

1. Introduction

Fuel cells are devices that can efficiently convert chemical energy to electricity. They can operate using different fuels (i.e. methanol, H_2), with hydrogen being the one most commonly used. The use of hydrogen as fuel is considered to be environmentally friendly because, in such a case, the only emission is water. Unfortunately, H_2 does not exist as a pure compound on earth. As a result, it must be produced either from electrolysis of water or conversion of hydrocarbons (i.e. biofuels, natural gas, diesel, etc.). Issues related to H_2 storage and distribution have rendered on-site H_2 production an attractive alternative solution, especially for automotive applications. Steam reforming, autothermal reforming and partial oxidation are three important processes for the conversion of hydrocarbons to H_2. The H_2 streams produced from the above reactions contain significant amounts of CO, which is undesirable because it poisons the fuel cell catalyst. One way to reduce the CO concentration is the water gas shift (WGS) reaction:

$$CO + H_2O \leftrightarrow CO_2 + H_2, \quad \Delta H_{RXN} = -41.4\,kJ/mol$$

WGS is a reversible exothermic reaction, thus high temperatures which favor fast kinetics are not suitable for achieving high conversions. One novel approach for improving the performance of WGS is the implementation of catalytic membrane reactors. Such reactors combine reaction and separation into one unit. A catalytic membrane reactor that allows the selective removal of one of the WGSR products (H_2 or CO_2) is expected to increase the CO conversion at high reaction temperatures.

In the past, several research groups have compared the performance of a membrane WGS reactor to that of a conventional reactor. In most cases, H_2 selective membranes such as Pd [1], Ag–Pd alloys [2], or microporous silica [3–5], and/or porous vycor glass [6] have been tested. Recently, studies using CO_2 selective membranes have also appeared in literature [7–9]. The findings indicate that a WGS membrane reactor is expected to have enhanced performance in terms of CO conversion compared to that of a conventional reactor.

In addition to experimental studies, many research groups have tried to simulate WGS membrane reactors. A WGS membrane reactor was first simulated using a simplified model that considered a membrane with Knudsen permeability [10]. The model also assumed the feed gas stream was continuously at equilibrium (fast WGS kinetics). As a result, the composition of the feed stream changed continuously as each gas permeated through the membrane at a different rate. It was found that under isothermal conditions a multistage reactor module was needed in order to increase the H_2 concentration beyond 90%.

A series of articles have presented experimental results and simulation studies concerning the performance of Pd or Pd–Ag based

* Corresponding author. Tel.: +30 2610965242; fax: +30 2610965223.
E-mail address: vnikolak@iceht.forth.gr (V. Nikolakis).

0376-7388/$ – see front matter © 2010 Elsevier B.V. All rights reserved.
doi:10.1016/j.memsci.2010.01.014

membrane WGS reactors. The main characteristic of these studies is that the membranes used were highly permselective for H_2, preventing the permeation of any other components. In particular, the effect of co-current vs. counter-current mode has been studied using a 2D model that takes into account radial dispersion by molecular diffusion [11]. The model predictions indicated only slight differences in terms of CO conversion between each operating mode, even though the axial profiles were different. On the other hand, they have found that it is possible to recover higher amounts of H_2 on the permeate side of the reactor in the counter-current mode of operation. The effect of the Damkhöler number at the inlet [4], the operating conditions (i.e. temperature, reaction pressure, feed flow rate) [12], and the catalyst mass distribution [13] on reactor performance has also been studied. It has been found that under certain conditions, using this type of reactor, it is possible to obtain almost 100% CO conversion [14].

Koukou et al. [5] have studied the effect of non-ideal flow effects (axial and radial dispersion) on the performance of an adiabatic packed bed membrane reactor. They used the parameters of a microporous silica membrane with H_2 permselectivity of ~15 and the Power Law type reaction rate expression for a Fe–Cr catalyst. The CO conversion and H_2 recovery predictions using simulations that took into account the dispersion were lower than the predictions made using a simplified plug-flow model.

Ma and Lund [1] have studied an adiabatic packed bed Pd-based membrane reactor. Among other parameters, they have assessed the effect of the CO_2 rate inhibiting effect on reactor performance. They have found that for iron–chrome catalysts the elimination of the CO_2 inhibitory effect is more important in enhancing the reactor performance than the equilibrium shift due to H_2 removal.

Alfadhel and Kothare [15] have developed a detailed mathematical microfluidic model for a membrane microreactor. The model uses the Navier–Stokes equations and incorporates reaction, and membrane permeability, as well as the possibility of having slipping flows.

Huang et al. [7,16] have investigated the possibility of using a CO_2 selective membrane to enhance the CO conversion and to increase the H_2 purity on the high pressure side of the membrane reactor. The effect of operating parameters such as feed concentration, temperature and pressure, as well as membrane permselectivity, has been investigated. The modeling results have shown that it is possible to recover more than 97% of the H_2, with ~10 ppm CO, by adjusting the operating parameters.

The studies mentioned above have clearly shown the potential benefits of utilizing a WGS membrane reactor. However, most of the studies have focused on one particular membrane (i.e. Pd or Pd–Ag based membranes) which has pre-set characteristics (i.e. permeability and permselectivity). Until today, only a few parametric studies have appeared that examine the effect of relative values of permselectivity, permeation rate, and reaction rate on membrane reactor performance [17]. Furthermore, these studies have focused primarily on dehydrogenation reactions. An in depth understanding of the effect of all these parameters on reactor performance is expected to provide guidance for developing new membrane materials.

The goal of this publication is to understand the effects of several WGS membrane reactor design and operational parameters on its performance. Two dimensionless numbers, namely Damkhöler (*Da*), and permeation (*Pe*), have been used to describe the relative reaction and permeation rates. The values of *Pe* and permselectivity have been selected based on the performance of SiO_2 membranes reported in the literature. We have not used data from Pd-based membranes because they have lower *Pe* values, and as a result they require higher feed pressures in order to achieve the same permeation flux. Furthermore, the membrane permselectivity, as well as the effect of using a CO_2 selective vs. an H_2 selective membrane, have been examined in relation to the WGS reaction mechanisms. For these reasons, several mechanisms (i.e. Langmuir–Hinshelwood or Redox) have been tested. Finally, the effect of using or not using a sweep gas has also been examined.

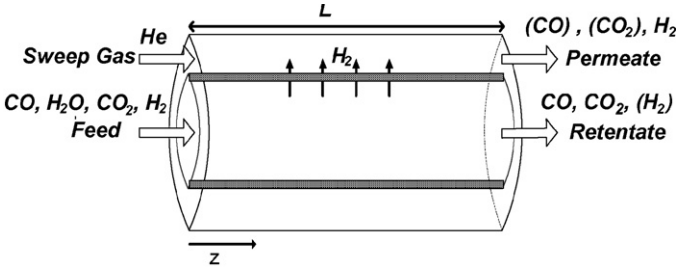

Fig. 1. Schematic representation of the membrane reactor modeled.

2. The reactor model

The membrane reactor modeled had a typical tube–shell geometry (Fig. 1). The inner tube is porous (membrane) and the outer tube is impermeable. The reactants were fed into the tube side of the reactor, while a sweep gas was fed into the shell side. The catalyst has been deposited as a thin layer on the inner side of the membrane and, as a result, only the gases at the tube side were in direct contact with it and participated in the reaction.

The mathematical model has been developed assuming the following:

1. Isothermal operation at steady state.
2. No radial concentration distributions in the tube or on the shell side of the reactor.
3. Plug flow in both compartments of the reactor (no axial mixing).
4. Permeation through the membrane is proportional to the difference in the partial pressure of each component between the tube and shell side.
5. The catalyst layer is an infinitely thin layer on the inner side of the tube.
6. Negligible effect of competitive reactions.
7. Ideal gas behavior.

The equations used and the corresponding boundary conditions are presented in Table 1.

The majority of the calculations have been carried out using a simple reversible reaction that corresponds to the catalyst Cu/ZnO ((R1) of Table 2), using the reaction rate constant from the literature [18]. Numerous studies concerning WGS reaction kinetics have been published so far. It is generally accepted that the WGS proceeds via either a Langmuir–Hinshelwood (L.H.), redox or Eley–Rideal type mechanism. Depending on the mechanism and the rate limiting step, the reaction rate expressions have different dependences on the partial pressures of the compounds participat-

Table 1
Differential equations and boundary conditions for the tube side and shell side of the reactor.

Tube side	Shell side
(1) $\frac{dF_i^{tube}}{dz} \pm r_i \frac{m_{cat}}{L} + Q_i \Delta P_i \frac{Area_{membrane}}{L} = 0$	(6) $\frac{dF_i^{shell}}{dz} - Q_i \Delta P_i \frac{Area_{membrane}}{L} = 0$
(2) $\frac{dP_{tube}}{dz} = -\frac{8\bar{u}\mu_{mix}}{r_{support}^2}$	(7) $\frac{dP_{shell}}{dz} = \frac{-8\bar{u}_p\mu_{mix}}{r_k^2}$
(3) $u[z] = \frac{RT/P \sum F_i^{tube}}{S}$	(8) $u_{Shell}[z] = \frac{RT/P \sum F_i^{shell}}{S}$
(4) $F_i^{tube}[z=0] = F_{i,0}^{tube}$	(9) $F_i^{shell}[z=0] = F_{i,0}^{shell} = 0$
(5) $P_{tube}[z=0] = P_{in}$	(10) $P_{shell}[z=0] = P_{shell,in}$

Table 2
Expressions of the WGS rate reaction kinetics, and of the parameter temperature dependence used in the simulations ($\beta = (P_{CO_2}P_{H_2})/(K_{eq}P_{CO}P_{H_2O})$).

Rate expression		Kinetic parameters	References
$r_{CO} = K\left(P_{CO}P_{H_2O} - \frac{P_{H_2}P_{CO_2}}{K_{eq}}\right)$	(R1)	$K = 82.2e^{-47{,}400/T}$	[18]
$r_{CO} = \frac{KP_{CO}P_{H_2O}(1-\beta)}{\left(1 + K_{CO}P_{CO} + K_{H_2O}P_{H_2O} + K_{H_2}P_{H_2} + K_{CO_2}P_{CO_2}\right)^2}$	(R2)	$K = 0.92e^{-454.3/T}$ $K_{CO} = 2.2e^{101.5/T}$ $K_{H_2O} = 0.4e^{158.3/T}$ $K_{H_2} = 0.05e^{1596.1/T}$ $K_{CO_2} = 0.0047e^{2737.9/T}$	[19]
$r_{CO} = \frac{KP_{CO}P_{H_2O}(1-\beta)}{\left(1 + K_{CO}P_{CO} + K_{H_2O}P_{H_2O} + \left(K_{H_2}P_{H_2}\right)^{1/2} + K_{CO_2}P_{CO_2}P_{H_2}^{1/2}\right)^2}$	(R3)	$K = 2.391 \times 10^7 e^{-6949.2/T}$ $K_{CO} = 0.0942e^{1782.1/T}$ $K_{H_2O} = 0.0333e^{2088.8/T}$ $K_{H_2} = 0.0315e^{2057.7/T}$ $K_{CO_2} = 0.00314e^{3003.5/T}$	[20]
$r_{CO} = \frac{K(P_{H_2O} - (P_{CO_2}P_{H_2}/K_{eq}(T)))}{1 + K_{CO}P_{CO_2}/P_{CO}}$	(R4)	$K = 2.012 \times 10^8 e^{-8681.3/T}$ $K_{CO} = 3.518 \times 10^{-3} e^{3203.9/T}$	[20]
$r_{CO} = \frac{KK_{CO}K_{H_2O}P_{CO}P_{H_2O}(1-\beta)}{\left(1 + K_{CO}P_{CO} + K_{H_2}^{1/2}P_{H_2}^{1/2}\right)^2\left(1 + K_{H_2O}^{1/2}P_{H_2O}^{1/2} + K_{CO_2}P_{CO_2}\right)}$	(R5)	$K = 3.7 \times 10^7 e^{-78{,}200/T}$ $K_{CO} = 94.4$ $K_{H_2O} = 12.2$ $K_{H_2} = 462$ $K_{CO_2} = 2.4$	[21]

ing in the reaction. As a result, some of those have been selected in order to illustrate the effects of the more complicated reaction rate expressions on the performance of the membrane reactor. Expression (R2) corresponds to a L.H. model with surface reaction being the rate limiting step. The parameters have been estimated for $Cu/ZnO/Al_2O_3$ catalyst [19]. A different study, using the same type of catalyst, has estimated the parameters of expressions (R3) and (R4) [20]. (R3) corresponds to a L.H. model with the rate limiting step being the reaction of adsorbed CO and water molecules to form adsorbed formate and atomically adsorbed hydrogen species. (R4) corresponds to a redox mechanism in which the rate limiting step is the reaction of the oxidized support with CO to form CO_2 and a reduced surface site. Expression (R5) has been derived to express the kinetics of a $Pt/CeO_2/Al_2O_3$ catalyst [21] using a L.H. model. The Pt provides adsorption sites for CO and the CeO_2 for water. Details about the rate expressions, and the temperature dependence of their parameters can be found in Table 2. The geometric characteristics of the reactor, as well as the range of operational parameters used, are presented in Table 3.

The performance of the reactor has been evaluated using the following three parameters:

1. The overall CO conversion:

$$X_{CO} = \frac{F_{CO}^{feed} - \left(F_{CO}^{permeate} + F_{CO}^{retentate}\right)}{F_{CO}^{feed}}$$

Table 3
Simulated reactor dimensions and operational parameters.

Operational parameters	
Temperature (K)	623
Mass of catalyst (g)	0–2 g
Feed composition	11% CO–38% H_2O–44% H_2–7% CO_2
Tube feed pressure (atm)	2
Shell feed pressure (atm)	1
Tube feed flow (cm^3/min)	140
Sweep gas feed flow, He (cm^3/min)	220
Reactor dimensions	
Length [cm]	10
Tube diameter [cm]	0.4
Shell diameter [cm]	2.54

2. The H_2 recovery, which is defined as the ratio of the H_2 flow at the permeate to the total H_2 product flow:

$$R_{H_2} = \frac{F_{H_2}^{permeate}}{F_{H_2}^{permeate} + F_{H_2}^{retentate}}$$

3. The mole fractions of H_2 and CO at the permeate and the retentate streams of the reactor.

To gain a better understanding of the results, they are presented as a function of the following three parameters:

a. Membrane permselectivity:

$$PS_{i/j} = \frac{Q_i}{Q_j}$$

b. The Damkhöler number ($Da = r_o(m_{cat}/F_o^{feed})$) calculated at conditions at the reactor feed. This dimensionless number is the ratio of the mass consumption (or production) due to the reaction, to the axial transport via convection.

c. The permeation number ($Pe = Q_{H_2}\Delta P_{H_2}^{tube}(Area_{membrane}/F_{H_2}^{feed})$), calculated for H_2 at conditions at the reactor feed. This dimensionless number is the ratio of the mass consumption (or production) due to transport through the membrane, to the axial transport via convection.

The model assumes the absence of axial and radial mixing in the reactor. To assess the degrees of mixing along the axial direction, the Peclet numbers for the tube and shell side have been calculated for each pair of gases:

$$Pe_r = \frac{\hat{u}L}{D_{i,j}} \quad (11)$$

The mutual diffusion coefficient of *i, j* has been estimated for all pairs of the multicomponent mixture using the procedure described in literature [22]. Depending on the pair of gases chosen, Pe_r at 623 K varied between 142 and 2630, indicating that the axial dispersion due to molecular diffusion can be ignored. The influence of radial mass transport on the degree of radial mixing in wall coated tubular reactors has been studied in the past [23,24]. For

laminar flow in tubes, it can be estimated from the dimensionless two-phase mass transfer time [23]:

$$\tau = \frac{11}{48}\frac{r_{\text{support}}\hat{u}}{LD_{i,j}} \quad (12)$$

For the CO–H_2O pair, τ has been estimated to be approximately 0.07. Simulations of non-reversible bimolecular reactions have shown that when $\tau < 0.1$, for all values of *Da*, conversion approximates the value calculated using a plug-flow reactor (PFR) model [23]. In our case, WGS is reversible and, as a result, the effect of radial gradients due to the reaction is expected to be smaller. On the other hand, the contribution of the membrane permeation is enhancing radial gradients, especially at high *Pe* numbers. However, the highest *Pe* number studied was ~2, indicating that the assumption of non-radial dispersion can be considered as a good first approximation.

3. Results and discussion

3.1. Effect of Da and Pe

The flow rates of CO, H_2O, H_2, and CO_2 along the membrane tube and shell sides are shown in Figs. 2 and 3 respectively. The membrane H_2 permselectivity was set equal to 10 and the *Da* and *Pe* were varied between 0 and 1.5.

For all combinations of *Da*, and *Pe* examined, the molar flow rates of all components on the shell side increased along the reactor axis. The use of sweep gas dilutes the shell side and, as a result, despite the co-current flow, there is a driving force for permeation over the

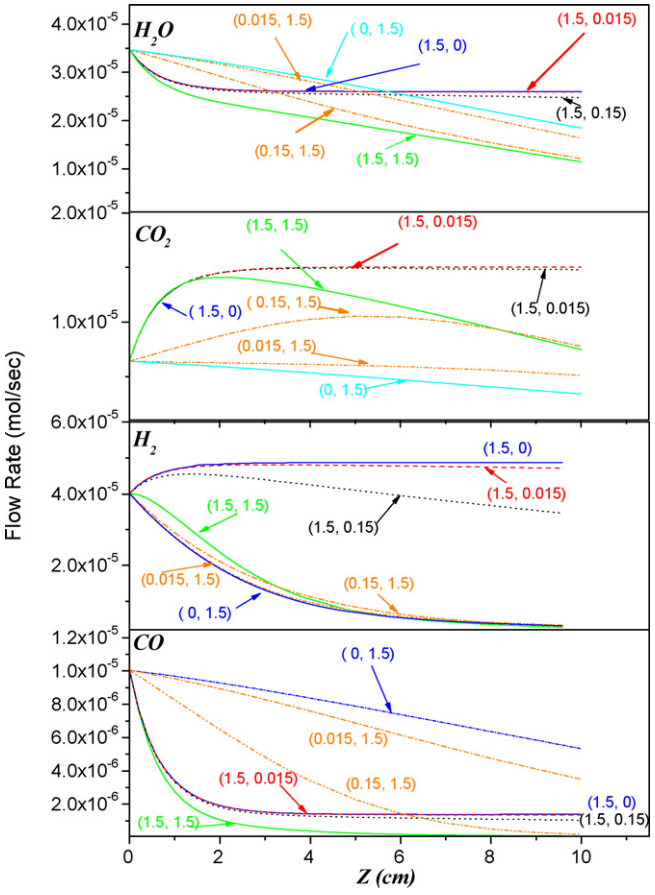

Fig. 2. Flow rates of H_2O, CO_2, H_2, and CO on the tube side of the membrane reactor along the axis of the reactor. Each line corresponds to a different combination of *Da* and *Pe* (for all simulations, H_2 membrane *PS* = 10).

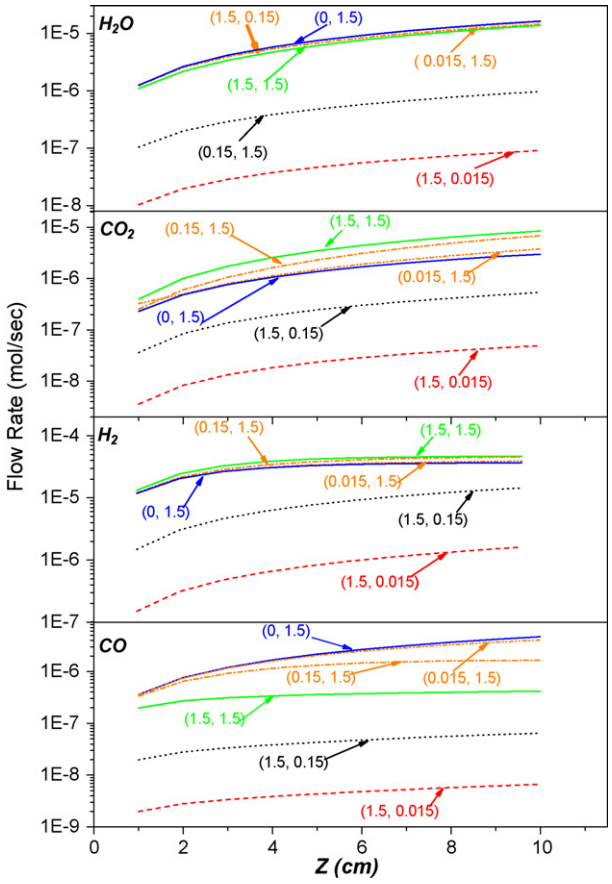

Fig. 3. Flow rates of H_2O, CO_2, H_2, and CO on the shell side of the membrane reactor along the axis of the reactor. Each line corresponds to a different combination of *Da* and *Pe* (for all simulations, H_2 membrane *PS* = 10).

entire membrane length. When *Da* = 0 and *Pe* = 1.5 (no reaction), the flow of each component decreased along the axis of the tube side due to permeation. The opposite was observed on the shell side. On the other hand, when *Da* = 1.5 and *Pe* = 0 (no permeation) the flows of CO and H_2O decreased and the flows of H_2 and CO_2 increased along the reactor axis, approaching a constant value as the reaction shifted towards equilibrium (after ~3 cm or ~30% of reactor length). These two combinations of *Da*, and *Pe* are two limiting cases corresponding to a membrane separator and a conventional tubular plug-flow reactor.

For all combinations of non-zero *Da* and *Pe*, the flow rates of CO and H_2O steadily decreased along the tube side of the membrane reactor. When *Da* > *Pe*, the molar flow rate of H_2 passed through a maximum. In the reactor axial segment before the maximum, the rate of H_2 production from the WGS reaction is higher than the rate of H_2 removal due to membrane permeation. The opposite is true in the segment after the maximum. The location of the maximum is at the point where these two rates become equal. A maximum is also observed in the CO_2 flow rate, for certain combinations of *Da* and *Pe* (i.e. *Da* = 0.15 and *Pe* = 1.5), due to the non-infinite values of H_2 permselectivity. Its location in the axial direction depends on the relative values of the H_2 and CO_2 mole fractions in the feed, as well as on the membrane permselectivity value. For H_2 selective membranes and feeds of low CO_2 content, it should occur after the maximum of the H_2 flow. When *Da* < *Pe*, the flow rate of H_2 decreased over the entire length of the reactor.

The most pronounced deviations from the two limiting flow profiles have been observed when *Da* = *Pe* = 1.5. The flow rate of H_2 was essentially constant close to the reactor feed and then gradually decreased following a profile similar to that of the mem-

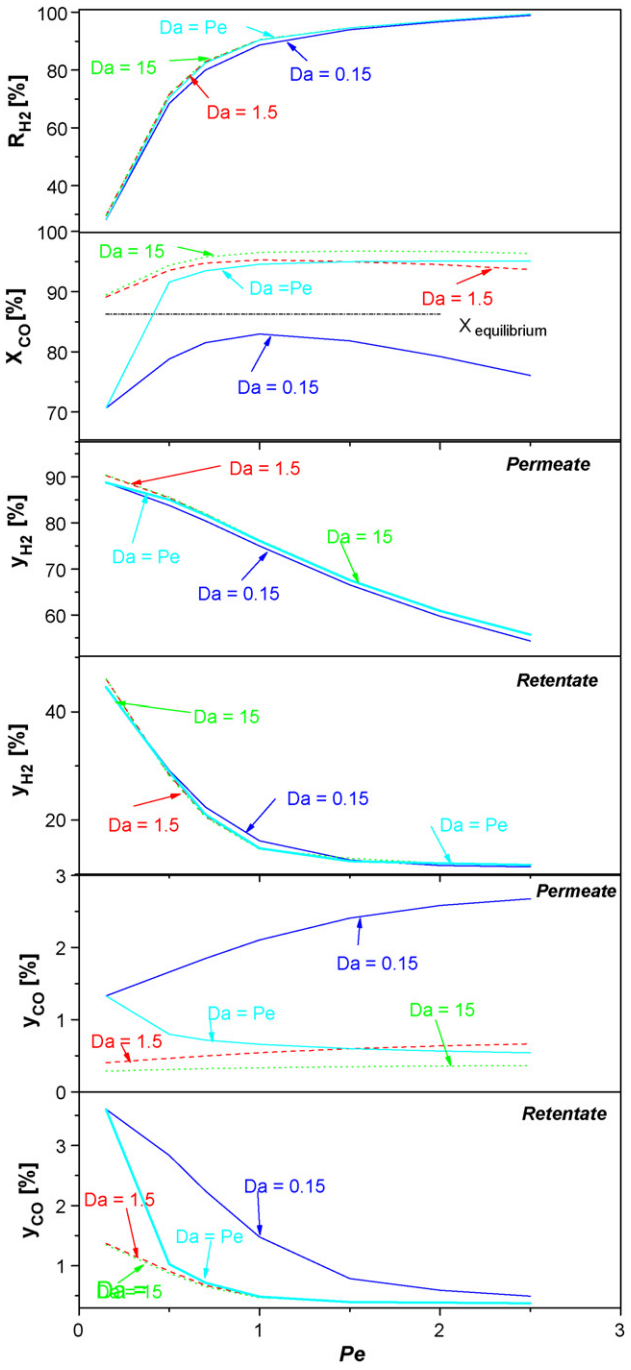

Fig. 4. CO conversion, H_2 recovery (top panels) and molar fractions of CO and H_2 at the reactor retentate and permeate (bottom panels) as a function of *Pe* for different values of *Da* (for all results, the H_2 membrane *PS* = 10).

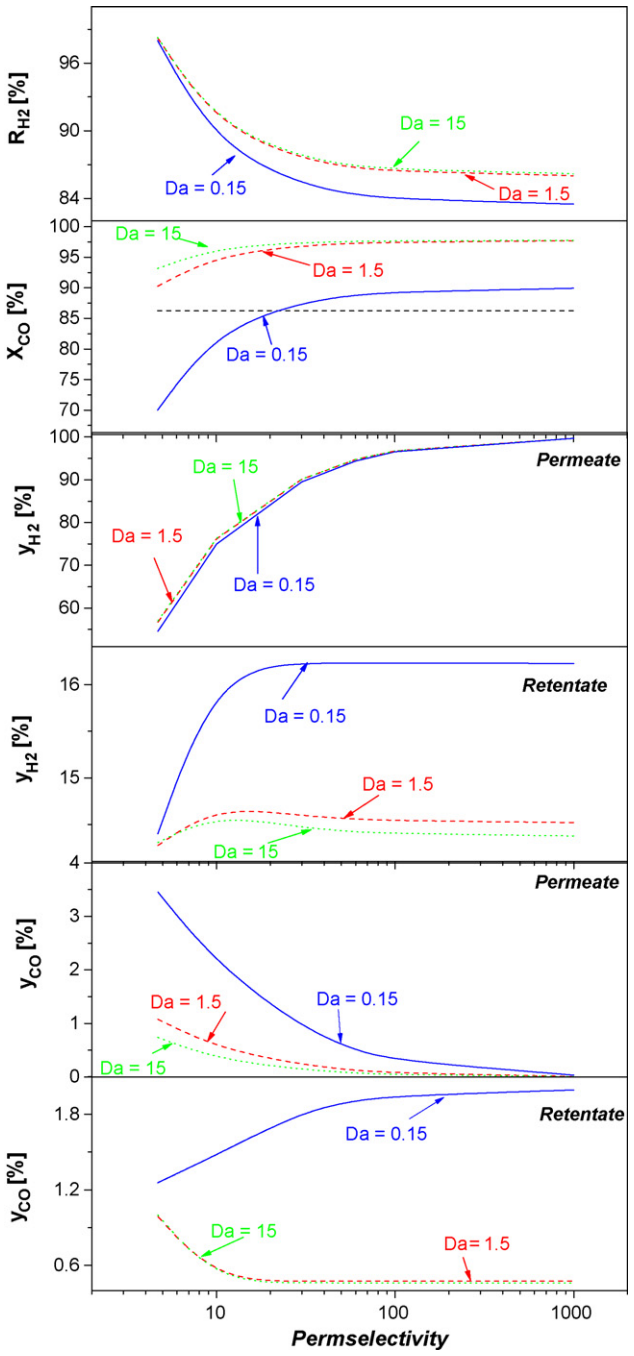

Fig. 5. Effect of membrane permselectivity on reactor performance. CO conversion, H_2 recovery (top panels) and molar fractions of CO and H_2 at the retentate and permeate (bottom panels) (for all simulations, *Pe* = 1).

brane separator. Furthermore, for this particular combination of *Da*, and *Pe*, the maximum decrease of CO and H_2O flow rates was observed.

The effect of *Da* on reactor performance as a function of *Pe* is presented in Fig. 4. In the same figure, the results from the case of *Pe* = *Da* are also presented. For all *Pe* values examined, conversion increases with *Da*. Similar results have also been reported by Tsuru et al. [25] in studies of methane steam reforming membrane reactors. On the other hand, for each value of *Da*, conversion passes through a maximum as a function of *Pe* that can be attributed to the permeation of reactants from the tube side to the shell side of the reactor before they react. This observation is due to the relatively low membrane permselectivity value (10) used in this particular simulation, and should not be observed if membranes with high H_2 permselectivity are used (i.e. Pd–Ag).

The conversion exceeded equilibrium for all *Pe* values tested when $Da \geq Pe = 1.5$. A tenfold increase of the *Da* from 1.5 to 15 improved conversion less than 1% when *Pe* was less than 1 and up to ~2% when *Pe* was more than 1. When the reaction is much faster than permeation, the composition on the tube side approaches the equilibrium value instantly, and the amount of steam and CO that permeate through the membrane before reacting is minimized. As a result, the conversion enhancement depends primarily on the product removal due to permeation. In contrast to CO conversion, H_2 recovery (Fig. 4) is primarily affected by the value of *Pe* and is

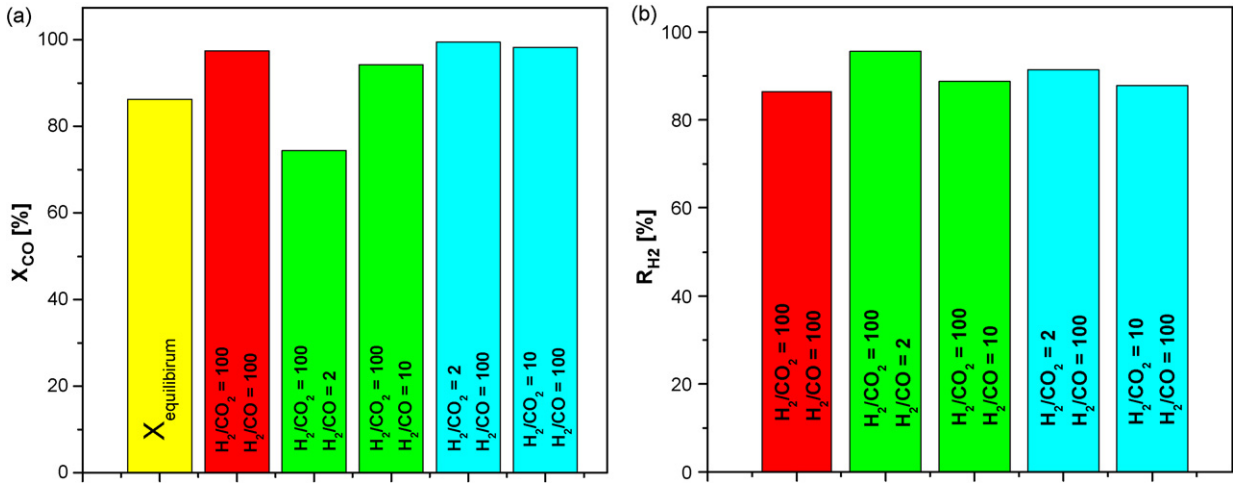

Fig. 6. Effect of H_2/CO_2 and H_2/CO permselectivity on membrane reactor performance: (a) CO conversion and (b) H_2 recovery.

almost insensitive to *Da*. In all cases, the partial pressure of all components on the shell side is very low due to the use of sweep gas. Furthermore, the differences in CO conversion (max ~20%) result in relatively small differences in H_2 concentration in the tube due to the low CO and high H_2 content of the feed (Fig. 4). As a result, the driving force for the H_2 permeation is primarily affected by *Pe* and not by the *Da* number. The CO mole fraction in both the tube and shell streams is affected by the value of both dimensionless numbers. The mole fraction of CO on the tube side decreased with *Pe*. Since the membrane is H_2 selective, the decrease can be attributed to the enhancement of the reaction. The opposite is observed on the shell side of the reactor. Based on the above, it can be concluded that there is a pair of *Da*, and *Pe* values that maximizes CO conversion; however, it is not possible to identify such a pair of values that simultaneously maximizes H_2 recovery, and y_{H_2}, and minimizes y_{CO}. This observation indicates that a MR utilizing a membrane with low permselectivity values could be beneficial in terms of improving CO conversion, but is highly unlikely to provide a single high purity H_2 stream without the need for further purification.

3.2. Effect of membrane permselectivity

Membrane performance as a function of membrane permselectivity, for $Pe = 1$ and for three different values of *Da*, is presented in Fig. 5. The CO conversion increased with membrane permselectivity, while the opposite was observed for H_2 recovery. It is interesting to note that high values of permselectivity resulted in conversions higher than equilibrium even for small values of *Da*. As mentioned in the previous section, a highly permselective membrane is expected to enhance conversion at smaller *Da* values because it prevents the permeation of reactants. Furthermore, the simulations indicate that increasing membrane permselectivity above 60 has only a slight influence on these two performance indicators. On the other hand, it has a pronounced effect on the H_2 and CO molar fractions on the shell side of the reactor. The purity of the H_2 on the shell side increases with permselectivity, reaching values above 99%. Furthermore, the CO mole fraction on the shell side decreases with increasing permselectivity, reaching values less than 0.01%. Taking into account that for LT-PEM fuel cells the CO concentration has to be less than 10–50 ppm, it should be possible to use the H_2 from the shell stream directly as fuel when the membrane permselectivity is above a certain value, which, for the parameters of the simulations shown here, is between 100 and 1000. For HT-PEM fuel cells, the mole fraction of CO must be less than 2%. The results shown here indicate that it is possible to achieve this target even if membranes with relatively low H_2 permselectivity values are used. Finally, it is interesting to note that y_{CO} on the tube side of the reactor increased with H_2 permselectivity when $Da = 0.15$. This observation is expected for a membrane separator and it indicates that, despite the selective removal of H_2, the reaction is not fast enough to consume the remaining CO.

The results presented above assumed H_2 permselectivity is the same for all compounds (CO, CO_2 and H_2O). This was done for simplicity. A real membrane material is expected to have different H_2 permselectivity values for each component. To examine this effect, we have varied the relative values of H_2/CO and H_2/CO_2 permselectivity, considering the value of 100 as the base case scenario (Fig. 6). When $PS_{H_2/CO}$ was higher than PS_{H_2/CO_2}, CO conversion was enhanced due to the selective removal of both reaction products. On the other hand, when $PS_{H_2/CO}$ was smaller than PS_{H_2/CO_2}, CO conversion decreased because a larger fraction of CO permeated through the membrane as well as because a larger fraction of the CO_2 produced remained on the tube side of the reactor.

3.3. Effect of feed stream composition

The feed composition shown in Table 3 has been selected as representative of a syngas reformate WGS reactor feed. One parameter that can be adjusted in this composition is the amount of steam. Simulations were carried out by varying steam to CO ratio between 1 and 4, keeping the molar ratio of the rest of the reactants constant. For each composition, the equilibrium conversion, the membrane reactor conversion, the H_2 recovery and $y^P_{H_2}$, y^P_{CO} are presented in Table 4. The equilibrium conversion and the conversion of the membrane reactor increased with the steam to CO ratio. The conversion improvement was more pronounced at low steam/CO ratios. In particular, when steam to CO ratio was 1, the

Table 4
Effect of H_2O/CO in the feed on equilibrium conversion, the membrane reactor conversion, the H_2 recovery and hydrogen and CO molar fractions at the permeate side. For all compositions the molar ratio of $CO/H_2/CO_2$ is 17.7/71/11.3, $Pe = 1$, $PS = 100$. $Da = 1.5$ for composition with $H_2/CO = 3.45$.

H_2O/CO in the feed	$X_{equilibrium}$ [%]	X_{CO} [%]	R_{H_2} [%]	$y^P_{H_2}$	y^P_{CO}
4	88.4	97.8	85.5	0.964	0.0037
3.45	86.3	97.5	86.4	0.967	0.0047
3	83.8	97.1	87.3	0.97	0.0061
2.5	80.1	96.5	88.3	0.973	0.0084
2	74.5	95.4	89.4	0.975	0.013
1.5	65.3	92.6	90.6	0.978	0.0019
1	50.0	81.3	91.6	0.98	0.0033

Table 5
Values of CO conversion and H_2 recovery for membrane reactors using an H_2 selective or CO_2 selective membrane, calculated using two different feed compositions.

Inlet composition [%] CO–H_2O–H_2–CO_2	Equilibrium conversion [%]	H_2 selective membrane		CO_2 selective membrane	
		X_{CO} [%]	R_{H_2} [%]	X_{CO} [%]	R_{H_2} [%]
11–38–44–7	86.3	98	87	95.9	2.4
20–20–10–50	59.3	75	75	83.2	3.7

conversion of the membrane reactor increased to 81% from 50% (equilibrium conversion of the feed composition). On the other hand, when the steam to CO ratio was 4, the conversion improved from 88.4% to 97.8%.

3.4. CO_2 vs. H_2 selective membranes

Recent developments in membrane science have indicated that it is possible to synthesize CO_2 selective membranes able to operate under conditions (temperature and humidity) encountered in water gas shift reactors (i.e. Li-glycinate polyvinyl alcohol) [8]. In this section, we are trying to present the effect of H_2 vs. CO_2 permselectivity on membrane reactor performance. The CO conversion and H_2 recovery values presented in Table 5 have been estimated for reactors having the same *Da*, and *Pe*, and permselectivity equal to 100. It must be noted that for the case of CO_2 selective membranes, *Pe* was calculated using the CO_2 feed mole fraction and permeance. Two feed compositions have been examined, one rich in H_2 and one in CO_2 [4]. For both compositions, H_2 recovery was higher in reactors using an H_2 selective membrane. On the other hand, small recoveries were estimated when a CO_2 selective membrane was used. From this perspective, utilization of CO_2 selective membranes might be advantageous since a large fraction of the H_2 product will be located on the tube side of the reactor, with a pressure close to that of the inlet stream. Such a configuration has the following potential benefits: (a) There is no need for an additional compressor, (b) the H_2 product is not diluted by the sweep gas, and (c) it is possible to recover the energy of this stream in a fuel cell stack.

When the H_2 content of the feed stream was higher than that of CO_2, the maximum conversion was obtained using an H_2 selective membrane. The opposite was observed when the CO_2 content of the feed was higher than that of H_2. This result was expected because CO_2 and H_2 have equal stoichiometric coefficients in WGS. Furthermore, unless the concentration of either H_2 or CO_2 is equal to zero, the reversible reaction will take place with a rate proportional to the product of the partial pressures of both components. The removal rate, due to permeation, of each component from the tube side of the reactor is proportional to the corresponding partial pressure difference between the tube and shell side of the reactor. As a result, when the concentration of H_2 (or CO_2) in the feed is small, the driving force for H_2 permeation will also be small, even if the membrane is H_2 permselective. Thus, it will not be possible to achieve high removal rates along the reactor tube. Consequently, the maximum removal of products is achieved when membranes that are permselective to the component (H_2 or CO_2) with the highest concentration in the feed are used.

3.5. Effect of reaction mechanism

To examine the effect of the different reaction mechanisms, shown in Table 2, on the MR performance, simulations were carried out using CO_2 and H_2 selective membranes for two different feed compositions (shown in Table 5), at two temperatures (623 K and 523 K). Each of the rate expressions shown in Table 2 corresponds to a catalyst with different activities. In order to compare the results, it is desired for all simulations to have the same value

Table 6
Effect of reaction mechanism on CO conversion and H_2 recovery at 623 K and 523 K, calculated using two different feed compositions. All simulations were carried out using *Pe* = 1 and *PS* = 100.

Rate expression	11% CO–38% H_2O–44% H_2–7% CO_2					20% CO–20% H_2O–10% H_2–50% CO_2				
	Da	H_2 selective membrane		CO_2 selective membrane		*Da*	H_2 selective membrane		CO_2 selective membrane	
		X_{CO} [%]	R_{H_2} [%]	X_{CO} [%]	R_{H_2} [%]		X_{CO} [%]	R_{H_2} [%]	X_{CO} [%]	R_{H_2} [%]
T = 623 K										
(R1)	1.5	97.5	86.8	95.9	15.6	1.5	79.1	84.0	82.2	3.0
(R2)	1.5	97.6	86.6	96.5	16.1	1.5	79.8	84.4	82.8	3.2
(R3)	1.5	97.4	86.5	95.9	15.9	1.5	79.3	84.3	81.9	3.1
(R4)	1.5	97.6	86.6	96.3	16.1	1.5	79.8	84.4	82.8	3.2
(R5)	1.5	97.6	86.7	96.7	16.2	1.5	80.1	84.4	83.1	3.3
T = 523 K										
(R1)	1.5	99.2	86.7	99.0	16.4	1.5	87.0	84.5	90.4	3.2
(R2)	1.5	99.4	86.8	99.0	16.5	1.5	89.6	84.8	91.7	3.5
(R3)	1.5	99.3	86.7	98.3	15.6	1.5	88.9	84.7	90.8	3.2
(R4)	1.5	99.4	86.8	98.9	16.1	1.5	89.8	84.8	91.8	3.5
(R5)	1.5	99.5	86.8	99.2	16.2	1.5	90.0	84.8	91.9	3.5
T = 623 K, *m* = 0.1 g										
(R1)	1.5	97.5	86.8	95.9	16.1	1.44	78.9	84.3	82.2	3.2
(R2)	0.20	97.2	86.4	94.8	15.8	0.16	72.9	83.4	79.8	2.9
(R3)	66.5	97.7	86.8	96.7	16.4	9.59	80.0	84.4	83	3.3
(R4)	39.9	97.7	86.8	96.7	16.4	8.13	80.0	84.4	83.2	3.2
(R5)	0.27	97.6	86.7	96.1	16.3	0.15	80.0	84.4	83	3.3
T = 523 K, *m* = 0.1 g										
(R1)	0.23	96.3	85.1	85.3	15.6	0.04	57.9	82.0	73.3	2.6
(R2)	0.11	98.8	86.3	96.2	15.6	0.08	65.8	82.5	82.7	2.7
(R3)	0.52	98.9	86.4	96.4	15.7	0.61	85.5	84.3	87.6	3.0
(R4)	1.18	99.4	86.9	98.8	16.3	0.25	88.6	84.8	91.2	3.3
(R5)	0.013	99.1	86.5	96.9	15.8	0.015	77.7	83.3	86.2	2.8

of *Da* at the reactor feed. This was achieved by adjusting the mass of the deposited catalyst. The results presented in Table 6 clearly indicate that different reaction mechanisms resulted in only slight differences in X_{CO} and R_{H_2} for each feed composition and at each temperature tested. This result might seem counterintuitive. Simulations carried out assuming an impermeable tube wall (conventional reactor) have shown that under the conditions examined all catalysts have reached the equilibrium CO conversion at less than 50% of the reactor length (Fig. 7). However, the axial position where the equilibrium conversion was reached was different for each rate expression. Furthermore, the MR simulations have shown that the X_{CO} axial profile is affected by the reaction rate expression only close to the reactor entrance. Then, for all mechanisms tested, it approached a similar value. This observation indicates that, once the composition on the tube side is close to the equilibrium, the reaction rate is primarily affected by the value of $(1-\beta)$ in the denominator, which has a value close to zero. X_{CO} and R_{H_2} calculated without adjusting the catalyst mass are also shown in Table 6. In that case *Da* varied between 0.15 and 66.5 at 623 K and between 0.013 and 1.18 at 523 K. The variations among calculated X_{CO} were higher than those observed when *Da* was kept constant. The biggest differences were observed at 523 K as a result of the low *Da* values calculated at this temperature.

Ma and Lund [1] have also carried out simulations of WGS membrane reactors and they have concluded that it is more important to synthesize improved catalysts for the high temperature WGS rather than improving the membrane's material performance. They have reached their conclusions taking into account the issue of CO_2 inhibition. However, in their study they have used parameters for Pd membranes that allow only H_2 permeation (infinite permselectivity). Our study indicates that if membranes with finite H_2 (or CO_2) permselectivity are used, there is an optimum value of *Pe* that maximizes the reactor performance. Furthermore, the issue of CO_2 inhibition can be addressed by utilizing CO_2 selective membranes, indicating that there is still room for research towards improving membrane material performance.

3.6. Effect of sweep gas

Finally, the effect of using a sweep gas on the shell side of the reactor has been examined for a reactor operating at 623 K with

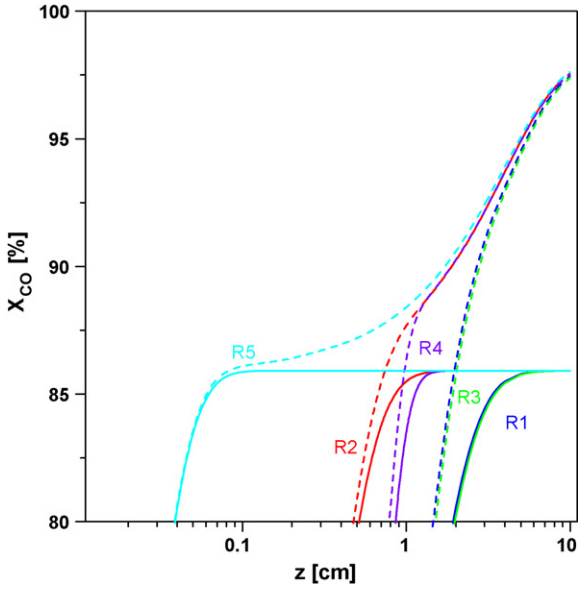

Fig. 7. Effect of reaction mechanism on CO conversion as a function of the reactor tube length (for all simulations, *Da* = 1.5, *Pe* = 1, and *PS* = 100).

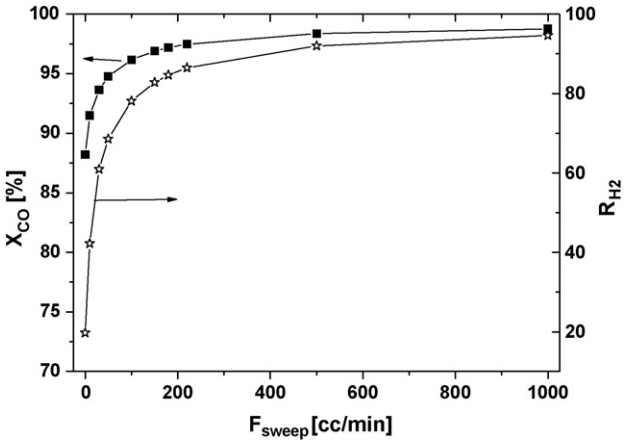

Fig. 8. Effect of sweep flow rate on CO conversion and H_2 recovery. Simulations were carried out at 623 K, using *Da* = 1.5, *Pe* = 1 and *PS* = 100.

Da = 1.5 and *Pe* = 1, and permselectivity equal to 100. As seen in Fig. 8, both X_{CO} and R_{H_2} increase with the flow rate of the sweep gas, approaching a constant value. Sweep gas has a significant effect on the reactor performance because it reduces the partial pressure of all components on the shell side of the reactor and enhances the permeation fluxes of all components. However, even though the utilization of a sweep gas is useful for evaluating a membrane reactor in lab scale experiments, it is not beneficial for industrial applications because an additional component is added to the system. Similar partial pressure differences between the tube and shell sides of the reactor can be achieved by either applying vacuum to the shell side of the reactor or by increasing the feed total pressure. Both of these operating modes are alternatives that can be applied to an industrial or pilot scale WGS membrane reactor.

4. Conclusions

The effect of WGS membrane reactor design and operational parameters on its performance has been studied by simulating the operation of an isothermal tube–shell reactor. In all cases the membrane performance was enhanced when a sweep gas was used on the shell side of the reactor. For all set values of reaction and permeation rates tested, CO conversion increased with membrane permselectivity. However, the most pronounced effect was observed for permselectivity values up to 60. Further increase of permselectivity resulted in only a slight improvement of CO conversion and H_2 recovery, however it increased the purity of the H_2 rich stream. When H_2/CO was higher than H_2/CO_2, the CO conversion was further improved due to the selective removal of both reaction products. For membranes with low permselectivity values (~10) it is shown that the maximum CO conversion is achieved when *Da* is almost equal to *Pe*. Utilization of such membranes in a membrane reactor can lead to enhanced conversions compared to conventional reactors, however they cannot provide a high purity H_2 stream without the need for further purification. The utilization of CO_2 selective, instead of H_2 selective, membranes could improve CO conversion only if the CO_2 content of the feed is higher than that of H_2. However, such configuration has the advantage that the larger fraction of the H_2 produced will be located on the high pressure tube side of the reactor. Finally, simulations using rate expressions that correspond to different detailed reaction mechanisms have shown only slight differences in CO conversions.

Acknowledgements

The authors would like to thank Prof. X.E. Verykios for fruitful discussions. P.B. acknowledges financial support of the "PENED-05/ΦΚΒ640" project which is cofunded: 75% public financing from the European Union—European Social Fund and 25% public financing from the Greek State, Ministry of Development—GSRT.

Nomenclature

$Area_{membrane}$	the membrane area [m^2]
Da	Damkhöler number
$D_{i,j}$	diffusion coefficient of gases i and j
F_i	molar flow rate of component i [mol s^{-1}]
F_i^{tube}, F_i^{shell}	molar flow rate of component i on the tube and shell side [mol s^{-1}]
$F_i^{permeate}$, $F_i^{retentate}$	molar flow rate of component i on permeate and retentate side [mol s^{-1}]
F_o^{feed}	inlet feed molar flow rate [mol s^{-1}]
$F_{o,i}^{tube}$	inlet molar flow rate in the tube [mol s^{-1}]
$F_{o,i}^{shell}$	inlet molar flow rate in the shell [mol s^{-1}]
K	reaction rate constant [mol s^{-1} m^{-2} kPa^{-2}]
K_{eq}	WGS equilibrium constant
K_i	adsorption constant of component i
L	reactor length [cm]
m_{cat}	mass of the catalyst [g]
P_{tube}, P_{shell}	the feed pressure on the tube and permeate side [kPa]
P_{in}	inlet feed pressure [kPa]
Pe	permeation number
Pe_r	Peclet number for tube and shell side
$PS_{i/j}$	membrane permselectivity
R	the ideal gas constant [atm cm^3 mol^{-1} K^{-1}]
Q_i	membrane permeance of component i [mol m^{-2} s^{-1} kPa^{-1}]
r_i	reaction rate [mol s^{-1} $g_{catalyst}^{-1}$]
r_o	reaction rate at the reactor entrance [mol s^{-1} $g_{catalyst}^{-1}$]
R_{H_2}	hydrogen recovery
r_k	the equivalent diameter of the annular orifice [cm]
$r_{support}$	the diameter of the membrane tube [cm]
S	the cross-sectional area of the tube or the orifice [cm^2]
T	the temperature [K]
$\hat{u}$	the average velocity on the feed side [m s^{-1}]
$\hat{u}_p$	the average velocity on the permeate side [m s^{-1}]
X_{CO}	CO conversion
y_i	molar fraction of species
z	axial coordinate [cm]

Greek letters

ΔP_i	trans-membrane partial pressure difference of component i [kPa]
μ_{mix}	viscosity of mixture [g cm^{-1} s^{-1}]
τ	two-phase mass transfer time

References

[1] D. Ma, C.R.F. Lund, Assessing high-temperature water-gas shift membrane reactors, Industrial and Engineering Chemistry Research 42 (2003) 711.
[2] V. Violante, A. Basile, E. Drioli, Composite catalytic membrane reactor analysis for the water gas shift reaction in the tritium fusion fuel cycle, Fusion Engineering and Design 30 (1995) 217.
[3] M.M. Abdel-jawad, S. Gopalakrishnan, M.C. Duke, M.N. Macrossan, P.S. Schneider, J.C. Diniz da Costa, Flowfields on feed and permeate sides of tubular molecular sieving silica (MSS) membranes, Journal of Membrane Science 299 (2007) 229.
[4] A. Brunetti, A. Caravella, G. Barbieri, E. Drioli, Simulation study of water gas shift reaction in a membrane reactor, Journal of Membrane Science 306 (2007) 329.
[5] M.K. Koukou, N. Papayannakos, N.C. Markatos, On the important of non-ideal flow effects in the operation of industrial-scale adiabatic membrane reactors, Chemical Engineering Journal 83 (2001) 95.
[6] S. Uemiya, N. Sato, H. Ando, T. Matsuda, E. Kikuchi, Steam reforming of methane in a hydrogen-permeable membrane reactor, Applied Catalysis 67 (1990) 223.
[7] J. Huang, L. El-Azzami, W.S.W. Ho, Modeling of CO_2-selective water gas shift membrane reactor for fuel cell, Journal of Membrane Science 261 (2005) 67.
[8] J. Zou, W.S.W. Ho, CO_2-selective polymeric membranes containing amines in crosslinked poly(vinyl alcohol), Journal of Membrane Science 286 (2006) 310.
[9] J. Zou, J. Huang, W.S.W. Ho, CO_2-selective water gas shift membrane reactor for fuel cell hydrogen processing, Industrial and Engineering Chemistry Research 46 (2007) 2272.
[10] A.S. Damle, S.K. Gangwal, V.K. Venkataraman, A simple model for a water gas shift membrane reactor, Gas Separation and Purification 8 (1994) 101.
[11] A. Basile, L. Paturzo, F. Gallucci, Co-current and counter-current modes for water gas shift membrane reactor, Catalysis Today 82 (2003) 275.
[12] G. Barbieri, A. Brunetti, T. Granato, P. Bernardo, E. Drioli, Engineering evaluations of a catalytic membrane reactor for the water gas shift reaction, Industrial and Engineering Chemistry Research 44 (2005) 7676.
[13] G. Chiappetta, G. Clarizia, E. Drioli, Theoretical analysis of the effect of catalyst mass distribution and operation parameters on the performance of a Pd-based membrane reactor for water-gas shift reaction, Chemical Engineering Journal 136 (2008) 373.
[14] A. Basile, G. Chiappetta, S. Tosti, V. Violante, Experimental and simulation of both Pd and Pd/Ag for a water gas shift membrane reactor, Separation and Purification Technology 25 (2001) 549.
[15] K. Alfadhel, M.V. Kothare, Modeling of multicomponent concentration profiles in membrane microreactors, Industrial and Engineering Chemistry Research 44 (2005) 9794.
[16] J. Huang, W.S.W. Ho, Effects of system parameters on the performance of CO_2-selective WGS membrane reactor for fuel cells, Journal of the Chinese Institute of Chemical Engineers 39 (2008) 129.
[17] W.S. Moon, S.B. Park, Design guide of a membrane for a membrane reactor in terms of permeability and selectivity, Journal of Membrane Science 170 (2000) 43.
[18] Y. Choi, H.G. Stenger, Water gas shift reaction kinetics and reactor modeling for fuel cell grade hydrogen, Journal of Power Sources 124 (2003) 432.
[19] N.E. Amadeo, M.A. Laborde, Hydrogen production from the low-temperature water-gas shift reaction: kinetics and simulation of the industrial reactor, International Journal of Hydrogen Energy 20 (1995) 949.
[20] J.L. Ayastuy, M.A. Gutierrez-Ortiz, J.A. Gonzalez-Marcos, A. Aranzabal, J.R. Gonzalez-Velasco, Kinetics of the low-temperature WGS reaction over a $CuO/ZnO/Al_2O_3$ catalyst, Industrial and Engineering Chemistry Research 44 (2005) 41.
[21] G. Germani, Y. Schuurman, Water-gas shift reaction kinetics over μ-structured $Pt/CeO_2/Al_2O_3$ catalysts, AIChE Journal 52 (2006) 1806.
[22] R. Krishna, R. Taylor, Multicomponent Mass Transfer, Wiley-IEEE, 1993.
[23] V. Balakotaiah, S. Chakraborty, Averaging theory and low-dimensional models for chemical reactors and reacting flows, Chemical Engineering Science 58 (2003) 4769.
[24] R.J. Berger, F. Kapteijn, Coated-wall reactor modeling-criteria for neglecting radial concentration gradients. 1. Empty reactor tubes, Industrial and Engineering Chemistry Research 46 (2007) 3863.
[25] T. Tsuru, K. Yamaguchi, T. Yoshioka, M. Asaeda, Methane steam reforming by microporous catalytic membrane reactors, AIChE Journal 50 (2004) 2794.